Case Studies in Construction Materials 19 (2023) e02640

Contents lists available at ScienceDirect

Case Studies in Construction Materials

journal homepage: www.elsevier.com/locate/cscm

Effect of carbonation duration on properties of recycled aggregate concrete

Long Li [a,b,c], Nazym Ziyabek [b], Yi Jiang [b,c], Jianzhuang Xiao [a], Chi Sun Poon [b,c,*]

[a] *Department of Structural Engineering, Tongji University, Shanghai 200092, PR China*
[b] *Department of Civil and Environmental Engineering, The Hong Kong Polytechnic University, Hong Kong*
[c] *Research Centre for Resources Engineering towards Carbon Neutrality, The Hong Kong Polytechnic University, Hong Kong*

ARTICLE INFO

Keywords:
Recycled aggregate concrete
Carbonation duration
Interface
Mechanical properties
Durability

ABSTRACT

The use of recycled coarse aggregate (RCA) produced from waste concrete in new concrete is an effective way to realize the recycling of construction and demolition waste. The utilization of accelerated carbonation to enhance RCA has attracted a lot attention because it can enhance performance of recycled aggregate concrete (RAC) and has potential for CO_2 sequestration. This study systematically investigated the influences of the duration of pressurized carbonation on the properties of RCA, RCA-new mortar interface, and RAC. The results showed that water absorption of carbonated RCA (CRCA) decreased with the increase of carbonation duration. But the beneficial effect of carbonation was less obvious after 1-day carbonation because most of calcium hydroxide and Ca-rich calcium silicate hydrates in RCA had reacted with CO_2 within 1 day. After using CRCA, the improvement in different performance indicators of RAC was dependent on different factors. The enhancement in compressive strength and chloride penetration resistance of RAC prepared with CRCA were dependent on the reduced porosity of CRCA. That was why they correlated with the water absorption of CRCA as carbonation duration increased. However, the decrease in initial absorption of water of RAC was mainly dependent on the denser surface layer of CRCA, rather than the reduced porosity of CRCA. This is because the denser surface layer can change water path from "penetrating through RCA" to "passing around RCA". It is recommended to use 1-day carbonation to enhance RCA, which might have higher cost-effectiveness.

1. Introduction

With rapid urbanization worldwide, especially in developing countries, a large amount of construction and demolition waste (C&DW) is produced, exerting heavy burdens on the limited landfilling capacities of city and worsening the environment. To reduce the amount of C&DW and save natural resources, new research and innovations have been implemented in the industry. One of them is the recycling of C&DW such as waste concrete to produce recycled coarse aggregate (RCA) and use it in new concrete. However, the properties of recycled aggregate concrete (RAC) are generally poorer in comparison to that of conventional concrete when the same water-to-cement (w/c) ratio is employed [1–5]. This phenomenon is linked to the inferior quality of RCA. Specifically, the porosity and water absorption of RCA are higher than that of natural coarse aggregates (NCA), and microcracks are present in RCA [6–9]. Due to these reasons, RCA are mostly used in non-structural applications [10]. However, in structural uses, the RCA replacement ratio in RAC

---

[*] Corresponding author at: Department of Civil and Environmental Engineering, The Hong Kong Polytechnic University, Hong Kong.
E-mail address: cecspoon@polyu.edu.hk (C.S. Poon).

https://doi.org/10.1016/j.cscm.2023.e02640
Received 14 August 2023; Received in revised form 16 October 2023; Accepted 1 November 2023

is strictly limited. For example, the maximum RCA replacement ratio in RAC is 20 % in the concrete specification of Hong Kong.

To promote the application of RCA, some pre-treatment methods were developed to improve the quality of RCA, including: (1) Removal of old mortar attached on RCA by mechanical grinding [11], microwave heating [12], acidic pre-soaking [13], etc.; (2) Enhancement of RCA by accelerated carbonation [14], polyvinyl alcohol pre-soaking [15], and so on; (3) Enhancement of the RCA-new mortar interface by coating nanoparticles [16] or cement slurry [17] on the surface of RCA; (4) Enhancing new mortar by using the techniques such as incorporating supplementary cementitious materials [18] or nanoparticles [19]. Among them, accelerated carbonation technologies such as gas-solid carbonation with or without pressure and wet carbonation, have attracted a lot of interest. That is because carbonation technologies can not only improve the quality of RCA, but also have potentials of CO_2 sequestration. The primary mechanism is that the cement hydration products such as calcium hydroxide (CH) and calcium silicate hydrates (C-S-H) in the old mortar of RCA would react with CO_2 to form calcium carbonate ($CaCO_3$), and it precipitates inside the pores and increases the solid volume, which leads to a decrease in porosity and water absorption [20].

By using carbonated RCA (CRCA), the properties of RAC are significantly enhanced [21–24]. There is no doubt that the densified RCA itself is one reason for the improved performance of RAC. Moreover, it was reported that using CRCA enhanced the bonding strength of the RCA-new mortar interface because $CaCO_3$ on the surface of CRCA could act as fillings and nucleation sites for the formation of additional C-S-H at the interface [25]. In addition, Wang et al. [26] reported that part of RCA was strengthened after carbonation, and the shell effect of the carbonated layer was a reason for enhanced durability, such as improved chloride penetration resistance and reduced sorptivity. However, there is no clear conclusion on which factor is the key to improving the mechanical properties and durability of RAC when incorporating CRCA.

It can be assumed that when the carbonation depth of RCA is small, the performance change is related to the strengthening new ITZ and the shell effect of carbonated surface layer. When the carbonation depth increases, the effect of RCA strengthening can also be linked to the performance enhancement of RAC. Therefore, by investigating the influence of carbonation duration, which is positively related to carbonation depth of RCA, we can understand which factor contributed more to the enhanced performance of RAC with CRCA. Although some studies [14,23] reported the effect of carbonation duration on the properties of RCA and performance of RAC, there is no systematic research on this topic from micromechanical properties to macro properties currently. Moreover, which factor contributed more to the enhanced performance such as strength, elastic modulus, sorptivity, chloride penetration resistance of RAC with CRCA is not well explained.

On another note, although increasing carbonation duration can increase the carbonation depth of RCA and enhance its physical properties, the macro-properties of RAC may only show limited improvement after a specific carbonation duration because the carbonation rate would be reduced. Therefore, it is necessary to study the effect of the carbonation duration of RCA on the performance of RAC to obtain an optimum carbonation time toward high cost-effectiveness.

In order to understand the key factor to the enhance performance of RAC when using CRCA, and optimum carbonation time toward high cost-effectiveness, this study will systematically investigate the effect of carbonation duration of RCA on the physical and microstructural properties of RCA, the bonding strength and microhardness of the interface between RCA and new mortar, and the macro properties of RAC.

2. Materials and methods

2.1. Materials

ASTM Type I Portland cement 52.5 N with a density of 3.15 g/cm^3 was used. The chemical composition of the cement is shown in Table 1. For the fine aggregate, river sand was employed and its fineness modulus was 2.6. The apparent density of the river sand was 2700 kg/m^3. The water was tap water. RCA was obtained by crushing mortar cubes (100 mm × 100 mm × 100 mm) at the age of 100 days. And then, the RCA were stored in the lab environment until the age of 6 month. The w/c ratio of the mortar cubes was 0.55, while the sand-to-cement ratio was 3.0. After crushing, the RCA with the size of 4.75–19 mm was obtained by sieving. According to the requirement on the grading of coarse aggregate in the standard ASTM C33/C33M-13, the mass ratio of particles with size of 4.75–9.5 mm to the particles with size of 9.5–19 mm is selected as 1/3. Additionally, mortar cubes with sizes of 40 mm × 40 mm × 40 mm were prepared as modelled RCA (MRCA) for assessment of the bonding strength between the MRCA and new mortar. The age of MRCA was same with that of RCA. The average compressive strength of the mortar cubes at age of 28 days was 40.2 MPa.

2.2. Carbonation process

A pressurized carbonation method was used in this study. The schematic of the carbonation chamber is shown in Fig. 1. Before carbonation, the RCA and MRCA were pre-conditioned by placing them in an environmental chamber (T = 25 ℃, RH=50 %) for 1-day, which would be the optimal condition for carbonation [27]. After pre-treatment, RCA and MRCA were cured in the carbonation

Table 1
Chemical composition of the cement.

Chemical compositions	MgO	Al_2O_3	SiO_2	P_2O_5	SO_3	K_2O	CaO	TiO_2	Fe_2O_3
Percentage in mass (%)	0.71	5.64	18.7	0.16	3.8	0.73	66.6	0.24	3.21

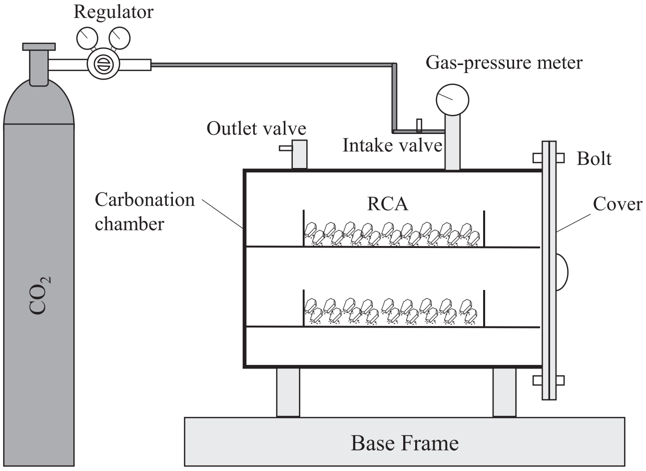

Fig. 1. Schematic of the pressurized carbonation chamber.

chamber for different ages, namely 1 h, 1 day, and 7 days. The untreated RCA and MRCA were named RCA-control and MRCA-control. The corresponding carbonated samples were designated as RCA-1 h-C, RCA-1d-C, RCA-7d-C, MRCA-1h-C, MRCA-1d-C, and MRCA-7d-C. During carbonation process, the pressure of CO_2 gas (> 99 % purity) in the chamber was controlled at about 1.0 Bar by a gas regulator, and the MgNO3 saturated solution was placed inside the chamber to control the moisture content at 65 % ± 5 %. The above carbonation conditions were referred to in the previous study [28] to promote carbonation efficiency.

2.3. Mix proportions and specimens

2.3.1. Specimens for testing the performance

Concrete specimens will be prepared using untreated RCA and CRCAs with different carbonation durations, and they were marked as RAC-control, RAC-1h-C, RAC-1d-C, and RAC-7d-C, respectively. The mix proportions of RACs are presented in Table 2. Considering that RCA can absorb water from new mortar, additional water was added to ensure the same effective W/C ratio was used. Here, the weight of the additional water was taken as the weight of coarse aggregate multiply the difference between water absorption and moisture content of coarse aggregate. The measured moisture contents of RCAs prepared with different carbonation durations were similar, and the values were about 2.24 %. The water absorption of RCA with different carbonation durations will be introduced in the results section. For each mix, 3 cubes with size of 100 mm × 100 mm × 100 mm were prepared for the compressive strength test, and 5 cylinders (Φ100 mm × 200 mm) were cast for the testing of stress-strain curve, sorptivity, and chloride penetration resistance.

2.3.2. Specimens for bonding strength test

The sample for testing the bonding strength between carbonated MRCA and new mortar is shown in Fig. 2. The procedures for preparing samples are shown as follows. First, for each type of MRCA, two cubes with size of 40 mm × 40 mm× 40 mm were placed in the middle of a mould with the size of 40 mm × 40 mm × 160 mm. Then, the new mortar was cast into the two sides of the mould. For the new mortar, the water/cement/sand ratio is 0.55/1/3. After curing for one day, demoulding was conducted and two samples for the bonding strength test (40 mm × 40 mm × 80 mm) were obtained. Finally, water curing was employed for the samples for 28 days before testing.

2.4. Test methods

Three series of testing were included in this study, namely the characteristics of RCA, the bonding strength and microhardness of the MRCA-new mortar interface, and the performance of RAC. The test methods implemented are introduced below.

Table 2
Mix proportions of RACs.

Mixture	Aggregate type	W/C ratio	Effective water (kg/m^3)	Additional water (kg/m^3)	Cement (kg/m^3)	Sand (kg/m^3)	Coarse aggregate (kg/m^3)
RAC-Control	Untreated RCA	0.60	210	65.2	350	736	1104
RAC-1h-C	RCA-1h-C	0.60	210	60.2	350	736	1104
RAC-1d-C	RCA-1d-C	0.60	210	51.7	350	736	1104
RAC-7d-C	RCA-7d-C	0.60	210	48.1	350	736	1101

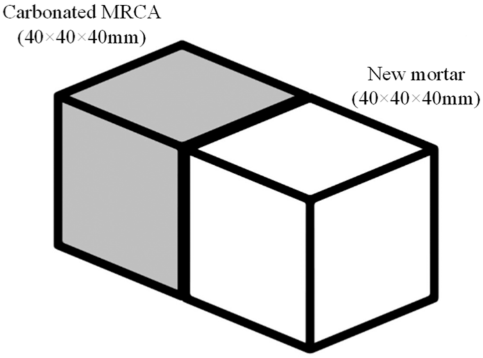

Fig. 2. Sample for testing the bonding strength between carbonated MRCA and new mortar.

2.4.1. *Methods for the characteristic of RCA*

The physical properties of RCAs with different carbonation durations including water absorption and particle density were measured according to the BS 812–2. Specifically, density on an oven dry basis, apparent density and density on a saturated and surface dry basis were measured.

The phase composition of the RCAs prepared with different carbonation durations were analysed by using thermogravimetric (TG, Rigaku, Thermo Plus EVO2), X-ray diffraction (XRD, Rigaku SmartLab 9 kW - Advance) and attenuated total reflectance -Fourier transform infrared spectroscopy (ATR-FTIR, PerkinElmer Spectrum Two). Before testing, the CRCA samples (<10 mm) were crushed to small particles, and then ground to less than 75 μm with an agate mortar. Finally, the samples were put in a vacuum oven (T = 40 ℃) for 7 days before testing. About 10 mg powdered sample was prepared for the TG test, and the temperature was risen from 40 ℃ to 1000 ℃ with a rate of 10 ℃/min under a nitrogen environment. In the XRD test, the prepared powdered sample was scanned from 5° to 70° with a step of 0.02° at 45 kV and 200 mA. The wavenumber of the ATR-FTIR pattern ranged from 400 to 4000 cm^{-1}.

The morphology of RCAs prepared with different carbonation durations were observed by a Tescan VEGA3 scanning electronic microscopy (SEM). The RCA samples with a size of less than 10 mm were selected. Before coating by gold for SEM testing, the RCA samples were put in a vacuum oven (T = 40 ℃) for 7 days for drying.

The micro-hardness was tested to evaluate the micromechanical properties of RCA samples prepared with different carbonation durations and to identify the carbonation depths. The procedures for preparing the sample for the microhardness test are shown as follows. First, samples with the dimension of around 20 mm × 20 mm × 10 mm were prepared by cutting from the MRCA sample. Then, the sample was dried in an oven (T = 60 ℃) for 1-day and fixed in epoxy resin using a cylindrical mould (Φ30 mm×30 mm). Finally, the surface of the sample for testing was ground and polished by using Buehler AutoMet 250 and then placed in a vacuum oven (T = 40 ℃) until testing. A digital Vickers Microhardness tester (HVX1000A, China) was used. In the test, the applying load was set to 0.098 N with a 10-second contact time. Indentations were made from the surface of the sample to the inner core side until the microhardness value showed no noticeable variation, which could cover the carbonated areas and uncarbonated areas. Then, the carbonation depth could be identified based on the results. To increase the accuracy of the data, five indentation points with an interval of 100 μm were selected at each distance from the surface of the sample.

In addition, phenolphthalein solution was used to identify further the carbonation depth of RCA prepared with different

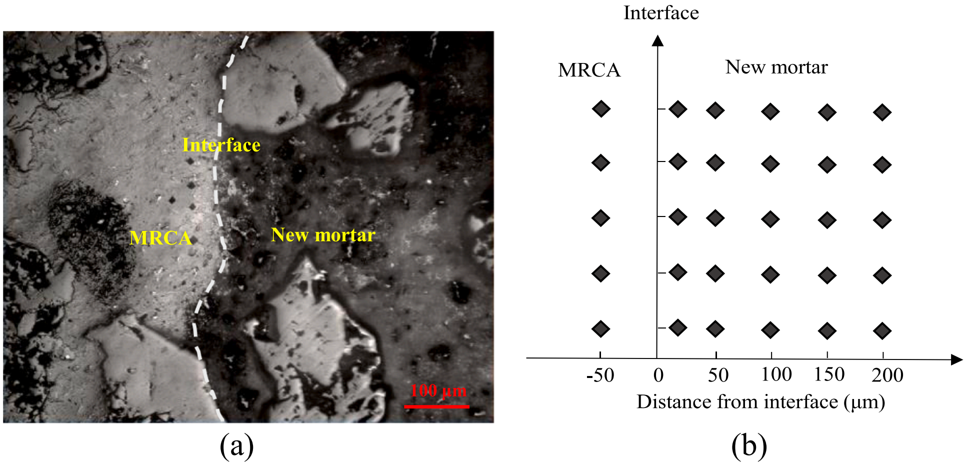

Fig. 3. A typical interface zone (a) and the selected indentation points (b).

carbonation durations. Immediately after removal from the carbonation chamber, the MRCA samples were split into two halves, and then the phenolphthalein solution was evenly sprayed on the fractured surface. The carbonation depth of RCA was identified by measuring the distance from the outer surface of the sample to the boundary of the pink area with a ruler. To increase the accuracy of the results, several samples of the same carbonation duration were measured, and the average result was reported.

2.4.2. Methods for the properties of the MRCA-new mortar interface

The bonding strength between MRCA prepared with different carbonation durations and the new mortar was measured using a direct tensile equipment. Before testing, the upper and lower faces of the samples were attached to the moulds for direct tensile strength with high-strength glue. During the testing, tensile loading was exerted on the specimens with a rate of 0.4 mm/min until the specimen fractured. Five samples were prepared for each group to obtain the average bonding strength.

The microhardness of RAC with CRCAs at the interface zone was evaluated. The sample preparation and loading pattern were similar to those described above. A typical interface zone and the selected indentation points in the microhardness test are shown in Fig. 3. On the MRCA side, the indentation points were located at −100 μm and −50 μm; while in new ITZ and new mortar side, the indentation points were located from 20 μm to 200 μm. At each distance, 5 indentation points were tested.

2.4.3. Methods for the properties of RAC

After mixing, the workability of concrete was assessed by the slump test based on the ASTM C143.

The compressive strength of RAC was measured based on the BS EN 12390-3. The size of RAC specimens was 100 mm × 100 mm × 100 mm. The loading rate was selected as 0.6 MPa/s. For each mix, three specimens were prepared to measure the average value.

The stress-strain curve of RAC was measured according to BS EN 12390-13:2013. For each mix, three cylinders with Φ100mm× 200 mm were prepared. The loading speed was 0.6 MPa/s during the test. The elastic modulus E was defined as:

$$E = (\sigma_1 - \sigma_2)/(\varepsilon_1 - \varepsilon_2) \tag{1}$$

Where, σ_1 and σ_2 are 5 % and 1/3 of the peak stress, respectively; ε_1 and ε_2 are the strain corresponding to σ_1 and σ_2, respectively.

The rate of absorption of water (sorptivity) of RAC was measured based on the ASTM C1585-13. Similar to the chloride penetration resistance test, three concrete cylinders (Φ100 × 50 mm) were prepared for each mix. The preparation of the samples was based on a previous study [28]. In this test, absorption (I) is defined as the change in mass divided by the product of the cross-sectional area of the specimen and the density of water. Based on the absorption-time ($I - \sqrt{t}$) curve, the rate of water absorption can be calculated. The initial rate of water absorption is the slope of the fitting line based on the data before 6 h in $I - \sqrt{t}$ curve. The secondary rate of water absorption is the slope of the fitting line based on the data after 6 h in $I - \sqrt{t}$ curve.

The chloride penetration resistance of RAC was measured based on ASTM C1202–19. For each mix, three concrete cylinders (Φ100 × 50 mm) were prepared by cutting from the cylinders (Φ100 × 200 mm). Each cylinder was fixed between two cells, which were filled with 3 % NaCl solution and 0.3 N NaOH solution separately. The charge passed was measured as the index of the chloride penetration resistance.

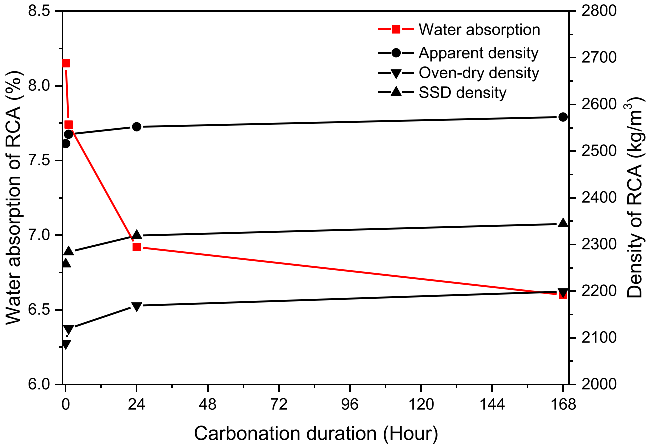

Fig. 4. Water absorption and density of RCA with different carbonation durations.

3. Test results and discussions

3.1. *Influence of carbonation duration on characteristics of RCA*

3.1.1. *Water absorption and density of RCA*

The water absorption and density of RCA prepared with different carbonation durations are displayed in Fig. 4. As the carbonation duration increased to 7 days, the water absorption of RCA decreased, while the densities of RCA increased. That is because CH and C-S-H could react with CO_2 to produce $CaCO_3$, which had a higher hardness and solid-phase volume that contributed to a decrease in porosity [29]. Moreover, with the increase of carbonation duration, the water absorption of RCA decreased more slowly, and the densities of RCA increased more slowly. E.g., when compared to uncarbonated RCA, the water absorption of CRCA after carbonation for 1 h, 1 day, and 7 days was reduced by 5.0 %, 15.1 % and 19.0 % respectively. In comparison, the dry particle density of RCA after carbonation for 1 h, 1 day, and 7 days was increased by 1.5 %, 3.9 %, and 5.3 % respectively. These phenomena indicated that the carbonation speed became slower with the increase in carbonation duration, especially after 1 day. On the one hand, that was because it was more difficult for CO_2 to penetrate the inner part of RCA (generally, the carbonation depth of concrete is proportional to $\sqrt{t}$ [30]. On the other hand, after 1 day of carbonation, most of the CH and high Ca/Si C-S-H (Ca-rich C-S-H) in RCA had reacted with CO_2 to form $CaCO_3$ and low Ca/Si C-S-H (Si-rich C-S-H). Although the Si-rich C-S-H could further react with CO_2, the carbonation rate would be much slower as carbonation rate of C-S-H decreases with the decrease of Ca/Si ratio [31].

3.1.2. *ATR-FTIR*

The ATR-FTIR results of RCA under different carbonation durations are presented in Fig. 5. The peaks assignment in FTIR-ATR results are shown in Table 3. In RCA-control, the peak at 965 cm^{-1} was related to the Si-O bond of the Q^2 unit of C-S-H [32]. After the carbonation, the peak gradually shifted to the left side. The peaks were located at 1005 cm^{-1} and 1034 cm^{-1} after carbonation for 1 h and 1 day, respectively, and the peak was stabilised at 1034 cm^{-1} after 1 day of carbonation. It was reported that with the decrease in the Ca/Si ratio, the peak of the Si-O bond in C-S-H shifted to a higher wave number. It indicates that during carbonation, C-S-H with a higher Ca/Si ratio (Ca-rich C-S- H) reacted with CO_2, producing $CaCO_3$ and C-S-H with a lower Ca/Si ratio (Si-rich C-S-H). Moreover, with the increase of carbonation duration from 1 h to 1 day, the intensity of the peaks corresponding to calcite, aragonite, and amorphous $CaCO_3$ increased obviously. After carbonation for 7 days, the intensity of the peak corresponding to calcite and aragonite was further increased. That was because the Si-rich C-S-H further reacted with CO_2 to produce $CaCO_3$ (calcite and aragonite) and calcium-modified silica gel [33].

3.1.3. *TG analysis*

The TG and DTG results of RCA prepared with different carbonation durations are displayed in Fig. 6. The peaks in the DTG curves can be assigned to four distinct phase-specific thermal events. The first peak at about 70 ℃ is related to the loss of moisture and the dehydration of C-S-H and ettringite (AFt). Because the RCAs were placed in an oven at 40 ℃ for 7 days, the presence of residual moisture could be neglected. The second peak at about 120 ℃ is due to dehydration of gypsum. The third band between 380 ℃ and

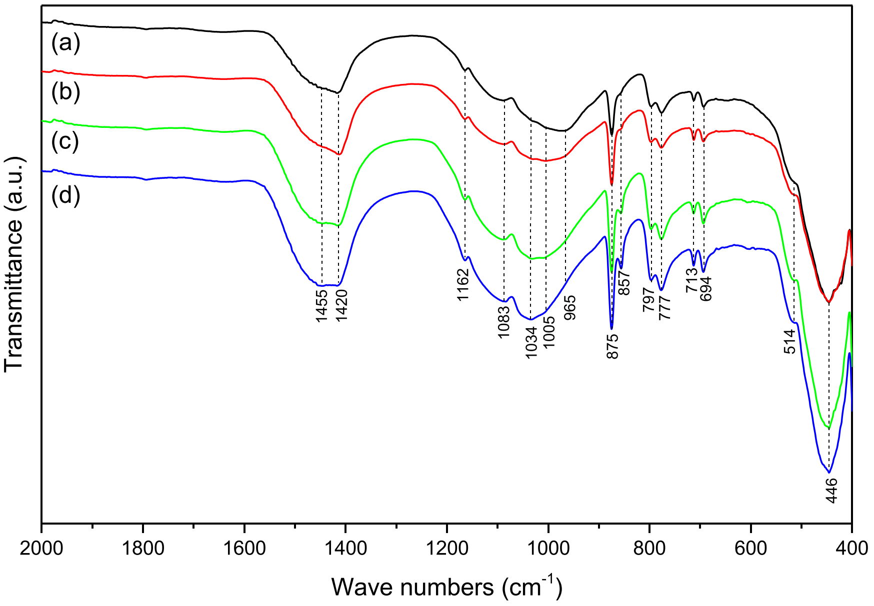

Fig. 5. ATR-FTIR results of RCA under different carbonation durations. (a) No carbonation; (b) 1 h carbonation; (c) 1 day carbonation; (d) 7 days carbonation.

Table 3
Assignment of ATR-FTIR bands.

ATR-FTIR Bands (cm^{-1})	Assignments	Reference
1420, 875,713	Calcite	[34]
857, 713, 1455	Aragonite	[35,36]
1460, 875	Amorphous $CaCO_3$	[37,38]
1083, 1162, 797, 777, 694, 514, 446	Quartz	[39]
965, 1005, 1034	C-S-H	[32]

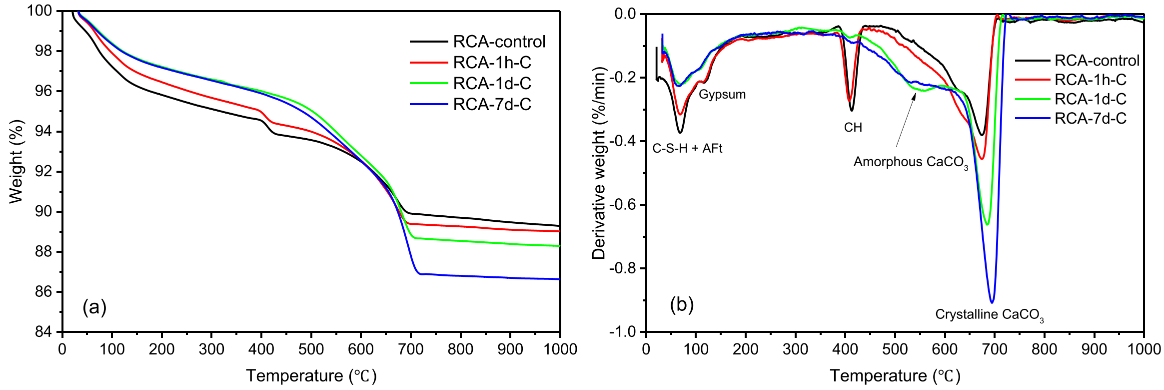

(a) (b)

Fig. 6. TG (a) and DTG (b) results of RCA with different carbonation durations.

430 ℃ is due to the decomposition of CH. The fourth band between 430 ℃ and730℃ is related to the decomposition of $CaCO_3$, which includes amorphous $CaCO_3$ (430 ℃~600 ℃) and crystalline $CaCO_3$ such as calcite and aragonite (600 ℃ ~ 730 ℃). The weight losses related to different minerals in RCAs are shown in Table 4. Here, the weight loss related to a specific mineral is defined as the weight loss at the range of the corresponding decomposition temperature. This method is to compare the relative content of specific phases, which has been used in previous study [40]. After carbonation for 1 h, the amount of C-S-H, AFt, and CH in RCA slightly decreased, and the amount of $CaCO_3$ slightly increased. After carbonation for 1 day, the CH and gypsum in RCA were almost all carbonated, and the amount of C-S-H continuously reduced. The amount of amorphous and crystalline $CaCO_3$ increased obviously. It indicates that both amorphous and crystalline $CaCO_3$ were produced during the carbonation of CH and Ca-rich C-S-H. After carbonation for 7 days, the amount of crystalline $CaCO_3$ continued to increase, while amorphous $CaCO_3$ did not show noticeable change. It was because part of Si-rich C-S-H, which was formed during the carbonation of Ca-rich C-S-H, further reacted with CO_2 to form crystalline $CaCO_3$.

3.1.4. XRD

The XRD results of RCA prepared with different carbonation durations can be seen in Fig. 7. Quartz, Calcite, CH, AFt, and gypsum were detected in RCA-control. After carbonation for 1 h, the corresponding sample RCA-1 h-C had a lower CH peak and a higher calcite peak. After carbonation for 1d, the peaks corresponding to CH and AFt disappeared, and the peak corresponding to gypsum was also not prominent. Instead, the peak corresponding to calcite increased, and the peaks related to aragonite could be detected. It suggested that CH, AFt, and gypsum had almost reacted with CO_2 within 1 day to form $CaCO_3$. After carbonation for 7 days, the peak corresponding to calcite further increased, which should be due to the continuous carbonation of Si-rich C-S-H. These results are consistent with the TG results.

3.1.5. Morphology of the surface of RCA by SEM

The morphologies of the surface of RCA prepared with different carbonation durations are shown in Fig. 8. C-S-H was the main phase observed on the surface of RCA-control. Also, no obvious CH was observed, but some small particles were observed, which might be assigned to amorphous $CaCO_3$ and calcite. That was because the CH on the surface of RCA might have been reacted with CO_2 during storing in air. It also explained why the morphology of the surface of RCA-1 h-C was similar to RCA-control. However, after carbonation for 1 day and 7 days, some needle-shaped and granular phases were observed, which might be assigned to crystalline $CaCO_3$ (both aragonite and calcite) due to the accelerated carbonation of the Si-rich C-S-H.

3.1.6. Microhardness of MRCA and carbonation depth

The microhardness results of MRCA prepared with different carbonation durations are shown in Fig. 9(a). In MRCA-control, the microhardness values across the sample were similar (about 35 HV0.01) from the surface to the inner part. In MRCA-1 h-C, the microhardness at the surface increased to 73.6 HV0.01 and then decreased with the increase of depth until 500 μm. In MRCA-1d-C, the

Table 4
Mass loss related to different minerals in RCA with different carbonation durations.

	(<200 ℃) Dehydration of C-S-H, AFt, and Gypsum (%)	(380 ℃ ~ 430 ℃) Decomposition of CH (%)	(430 ℃ ~ 600 ℃) Decomposition of amorphous $CaCO_3$ (%)	(600 ℃ ~ 730 ℃)) Decomposition of calcite (%)
RCA-control	4.28 %	0.79 %	1.36 %	2.65 %
RCA-1 h-C	3.55 %	0.76 %	1.84 %	3.19 %
RCA-1d-C	2.80 %	0.32 %	3.01 %	4.14 %
RCA-7d-C	2.80 %	0.40 %	3.09 %	5.62 %

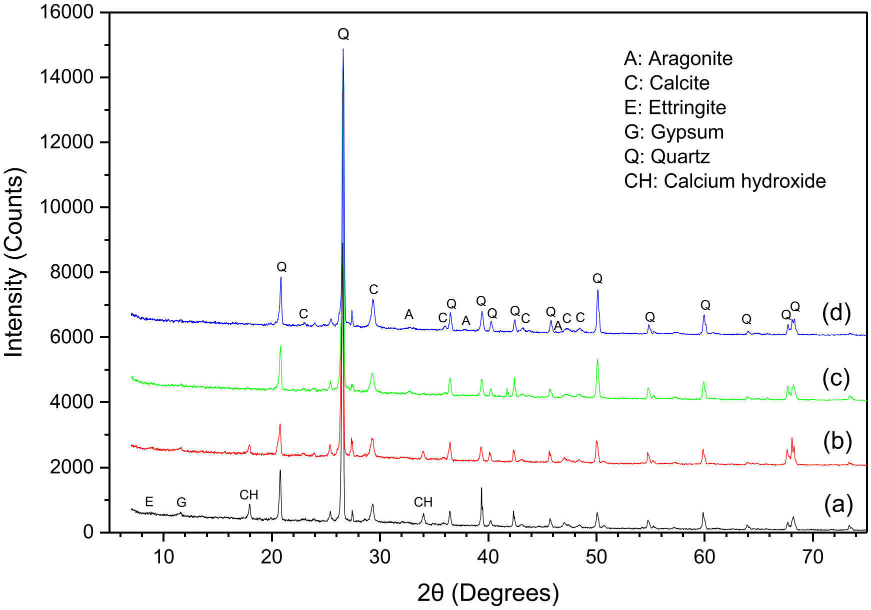

Fig. 7. XRD results of RCA under different carbonation durations. (a) RCA-control; (b) RCA-1 h-C; (c) RCA-1d-C; (d) RCA-7d-C.

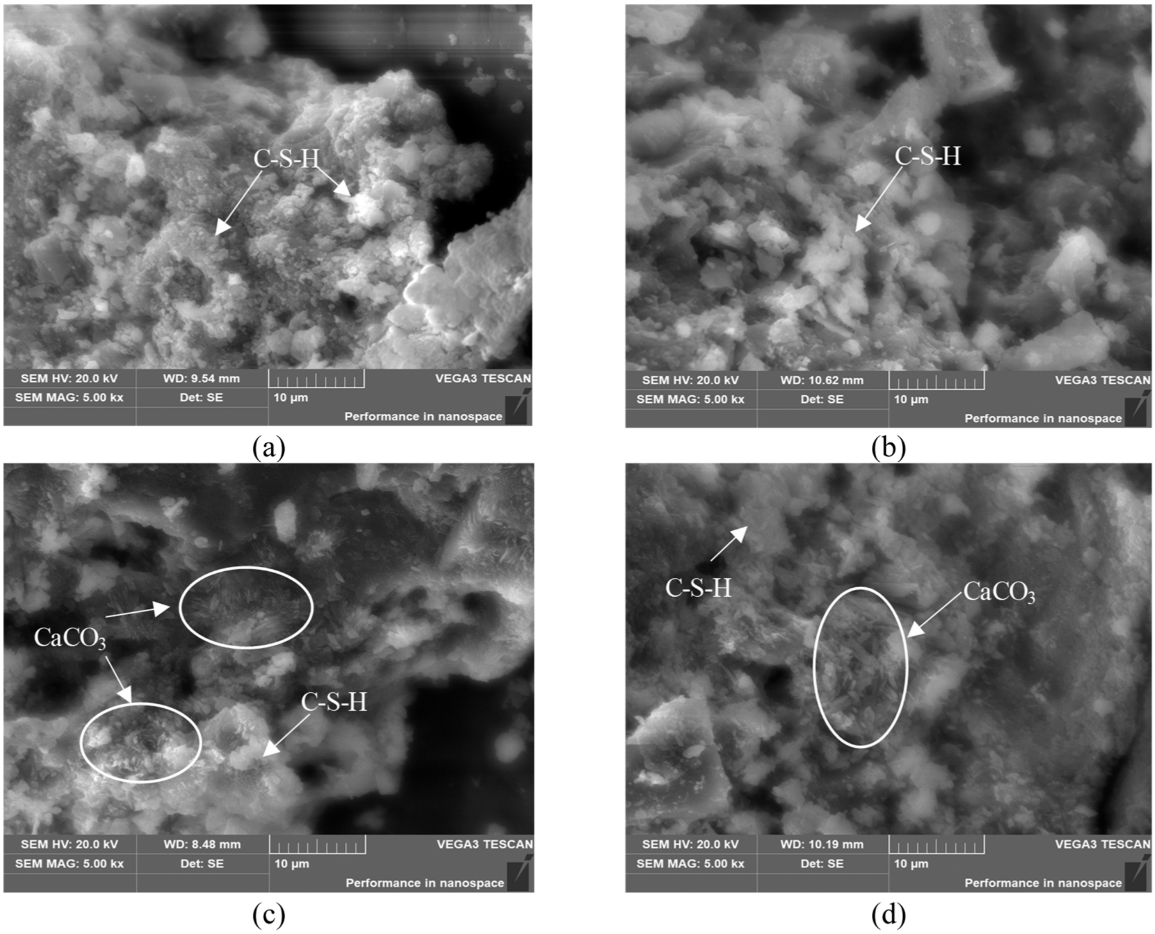

Fig. 8. Morphologies of the surface of RCA with different carbonation durations. (a) RCA-control; (b) RCA-1 h-C; (c) RCA-1d-C; (d) RCA-7d-C.

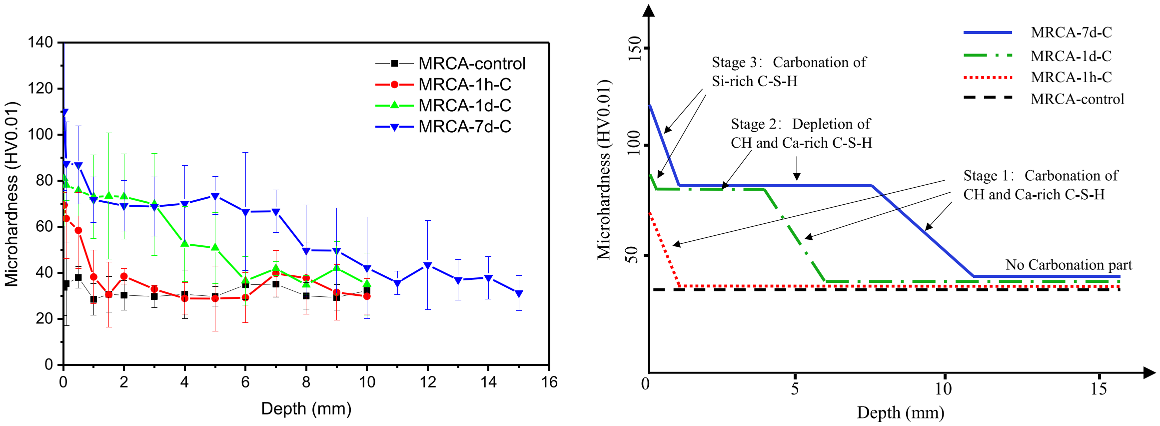

(a) Test results (b) Mechanisms

Fig. 9. Microhardness of MRCA with different carbonation durations.

microhardness at the surface layer increased to 80.9 HV0.01, and it remained at 73 HV0.01 before the depth of 3 mm. Then, the microhardness decreased gradually with the increase of depth until 6 mm from the surface. In MRCA-7d-C, the microhardness at the surface further increased to 110.1 HV0.01, and it decreased to about 73 HV0.01 at a depth of 1000 μm. Then the microhardness remained at this value until 7 mm before further decreasing. Based on the microhardness results and the previous analysis, the CO_2 diffused area in MRCA would experience three stages with the increase of carbonation duration:

- **Stage-1:** CH and Ca-rich C-S-H in the cement paste reacted with CO_2 to produce CC and Si-rich C-S-H, which increased the microhardness from about 35 HV0.01 to about 75 HV0.01.
- **Stage-2:** Carbonation of CH and Ca-rich C-S-H was completed. In this stage, the microhardness was stable at about 75 HV0.01.
- **Stage-3:** Si-rich C-S-H reacted with CO_2 to produce more crystalline CC such as aragonite and calcite and calcium-modified silica gel. In this stage, the microhardness increased from about 75 HV0.01 to 110 HV0.01.

The simplified microhardness results and the carbonation mechanism of MRCA prepared with different carbonation durations are shown in Fig. 9(b). In MRCA-1 h-C, only the surface layer (depth<0.5 mm) was under the stage-1 carbonation, and the degree of carbonation was higher as the carbonation depth was smaller. In MRCA-1d-C, CO_2 had diffused into the depth within 6 mm from the

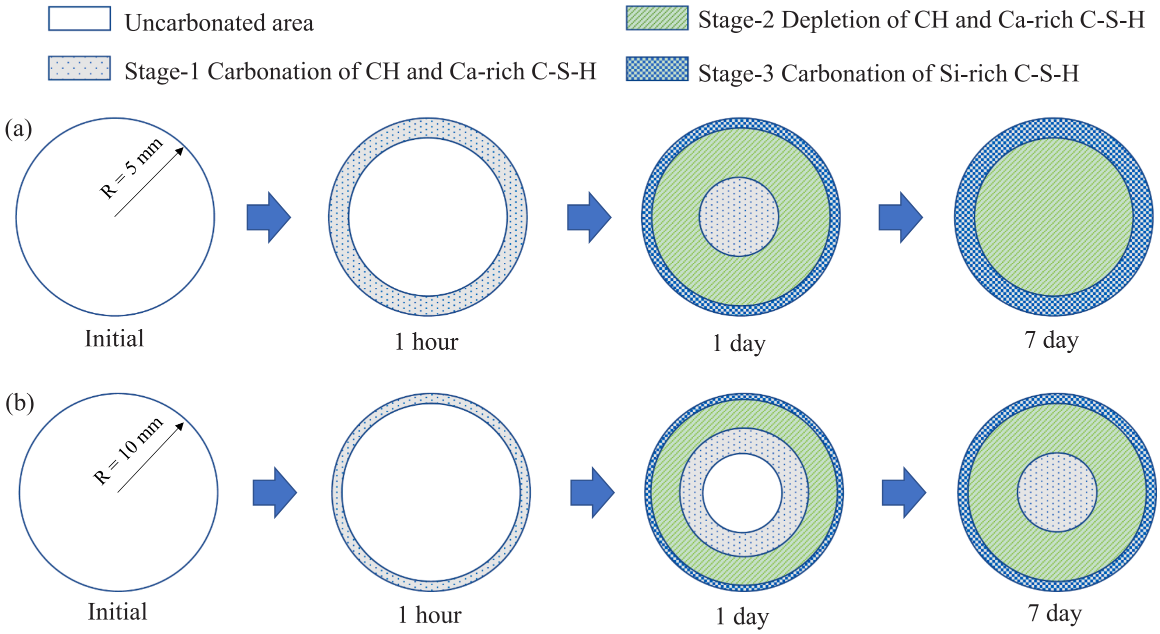

Fig. 10. Schematic of RCA under different carbonation durations. (a) RCA (d=10 mm); (b) RCA (d=20 mm).

surface. In the CO_2-diffused zone of MRCA-1d-C, the surface layer (depth<0.5 mm) was under the stage-3 carbonation, and the second layer (0.5 mm<depth<3 mm) was at the stage-2 carbonation, and the third layer (3 mm<depth<6 mm) was experiencing the stage-1 carbonation. In MRCA-7d-C, CO_2 gas had diffused into a depth of 11 mm from the surface. The surface layer (depth<1 mm) was experiencing stage-3 carbonation, the middle layer (1 mm < depth < 7 mm) was under stage-2 carbonation, and the stage-1 carbonation happened in the inner layer (7 mm < depth < 11 mm).

Based on the microhardness results of MRCA, the changes of RCA (e.g., d = 10 mm and d = 20 mm) with the increase of carbonation durations are analysed, as shown in Fig. 10. When the diameter of RCA is between 5 mm and 20 mm, most of the CH and Ca-rich C-S-H in RCA should have reacted with CO_2 after carbonation for 1 day. However, from 1 day to 7 days of carbonation, only a limited additional region was carbonated. This is the reason for the smaller enhancement of RCA properties after 1 day of carbonation.

In addition, the carbonation depth of CRCA could be estimated based on the microhardness results. The depth corresponding to the end of stage-1 carbonation could be considered the carbonation depth because CH and Ca-rich C-S-H had been depleted. From Fig. 9, the carbonation depth of MRCA-1 h-C, MRCA-1d-C, and MRCA-7d-C was 0 mm, 3 mm, and 7 mm, respectively. To confirm this, phenolphthalein solution was sprayed on the cross-section of the MRCA prepared with different carbonation durations, and the results are shown in Fig. 11. Normally, the area in pink represents an uncarbonated area. It can be seen that with the increase of carbonation duration, the carbonation depth increased, and the average carbonation depth of the MRCA were close to that determined from the microhardness results.

3.2. Influence of carbonation duration on the properties of RCA-new mortar interface

3.2.1. Bonding strength of the interface between MRCA and new mortar

The bonding strength between MRCA prepared with different carbonation durations and the new mortar are shown in Fig. 12. The bonding strength between the MRCA and new mortar increased with the increase of carbonation duration from 0 to 1 day. Compared to the control, the bonding strength using 1 h and 1-day carbonated MRCA increased by 20 % and 40 %, respectively. That was because the amorphous and crystalline $CaCO_3$ on the surface of CRCA could participate in the hydration reaction of new cement paste to form monocarbonates [25], which is beneficial for improving the chemical bonding between CRCA and the new mortar. However, the bonding strength between MRCA-7d-C and the new mortar showed a sudden decrease. There are two possible reasons for this phenomenon. On the one hand, the surface of MRCA-7d-C was too denser, and the free water could not penetrate the dense layer quickly. As a result, the free water near the interface accumulated, and the local w/c ratio increased, leading to a weaker ITZ. This is the so-called "wall effect". At the same time, as the surface of MRCA-7d-C became denser or less porous, the interlocking between the MRCA and the new cement mortar might be weakened. On the other hand, the surface of MRCA-7d-C was covered with primarily crystalline $CaCO_3$, which is less active than amorphous $CaCO_3$ formed because of shorter carbonation durations. As a result, it provided weaker enhancements on the chemical bonding between the MRCA and the new mortar.

3.2.2. Microhardness of the zone near the interface between MRCA and new mortar

The microhardness of the interface zone between the new mortar and MRCA with different carbonation durations are presented in Fig. 13. In the figure, the Y axis (x = 0) represents the interface between the MRCA and new mortar. The left-hand side was the MRCA, and the right-hand side was the new mortar. The results show that the microhardness of MRCA at the surface layer (within 100 μm) increased after carbonation and the MRCA-7d-C showed the highest value. The results agreed with the test results of MRCA in the previous section. When using MRCA-control, the microhardness had no noticeable change when the distance from the interface was between 20 μm and 200 μm in the new mortar. It means that there is no obvious weak ITZ between MRCA and the new mortar. When using the carbonated MRCAs, the phenomenon was similar. Moreover, the microhardness of the new mortar had no significant change, irrespective of whether using the uncarbonated raw MRCA or carbonated MRCA. It means that using the CRCA had limited influence on the properties of the new mortar.

3.3. Influence of carbonation duration on macro properties of RAC

3.3.1. Workability

The slump value of RAC prepared by using RCA with different carbonation durations are shown in Fig. 14. The results showed that

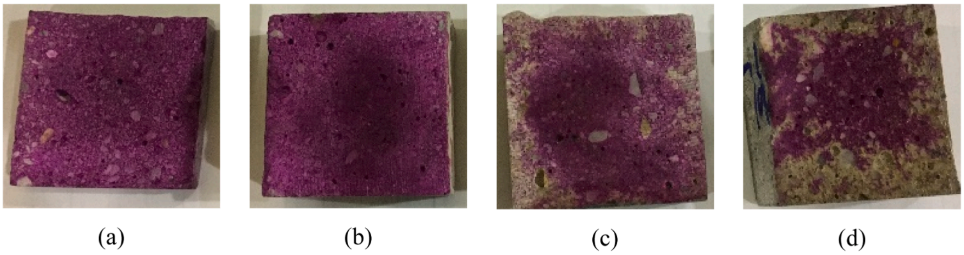
(a) (b) (c) (d)

Fig. 11. Cross section of MRCA (40 mm × 40 mm) with different carbonation durations after spraying phenolphthalein. (a) MRCA-control; (b) MRCA-1 h-C; c) MRCA-1d-C; (b) MRCA-7d-C.

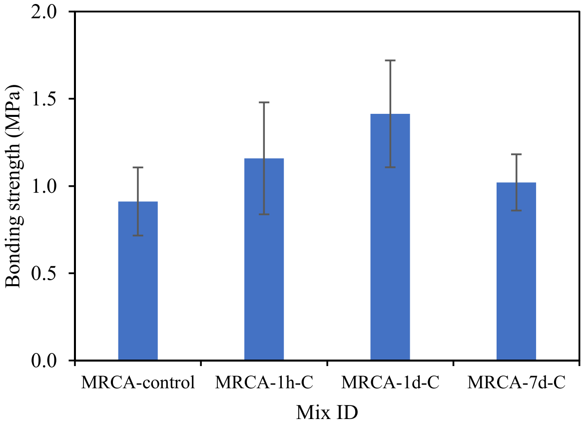

Fig. 12. Bonding strength of the interface between new mortar and MRCA prepared with different carbonation durations.

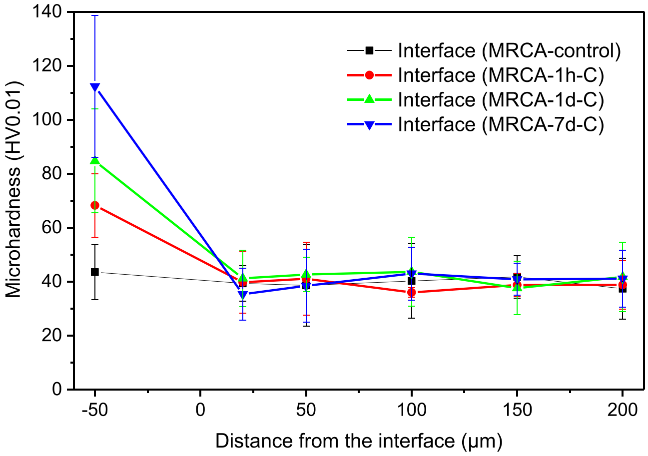

Fig. 13. Microhardness of interface zone between carbonated MRCA and new mortar.

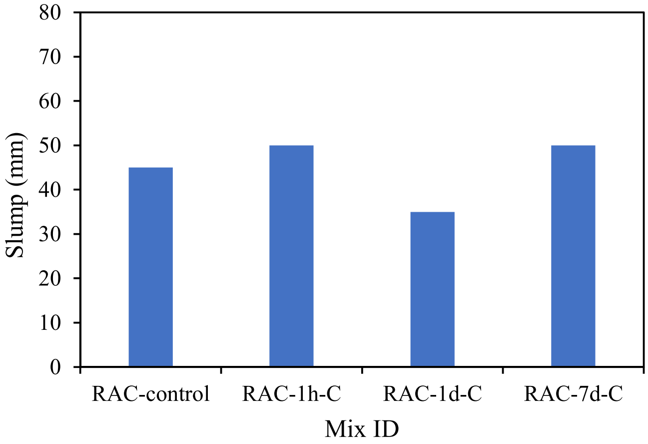

Fig. 14. Slumps of RAC using RCA with different carbonation durations.

the slump of RAC fluctuated irrespective of the different carbonation durations. It means that replacing uncarbonated RCA with the same amount of CRCA by mass did not influence the workability of RAC if the effective w/c ratio was kept the same. The possible reason is presented as follows. Initially, the amount of free water in RAC with uncarbonated RCA was higher than that using CRCA because more additional water was added. However, because the surface of the CRCA was denser than that of uncarbonated RCA, the uncarbonated RCA could absorb water faster from new mortar, which might offset the influence of the more additional water. As a result, the free water in new mortars prepared with different RACs was similar during the measurement of the workability. This was consistent with the fact that the microhardness of the new mortars was similar regardless of using uncarbonated RCA or CRCA.

3.3.2. Cube compressive strength

The compressive strength of RAC with CRCAs at age of 28 days are displayed in Fig. 15. With the increase of RCA carbonation duration to 7 days, the compressive strength of RAC increased. Compared to RAC-control, the increase of compressive strength of RAC-1 h-C, RAC-1d-C, and RAC-7d-C was 6.9 %, 18.9 %, and 22.5 %, respectively. It indicates that with the increase of carbonation duration, the compressive strength increased, but at a slower rate. Moreover, from 1 day to 7 days of carbonation, the compressive strength only increased by 3.6 %. This trend was similar to that of the water absorption test results of the RCA. The rate of increase in compressive strength of RAC prepared with CRCA increased approximately linearly with the decrease of water absorption of CRCA, as shown in Fig. 15(b). It indicates that the enhancement of RAC with CRCA was dependent on the reduction in the porosity of RCA. On another note, although the bonding strength of the interface between RCA-7d-C and the new mortar was lower than that using RCA-1d-C, the compressive strength of RAC-7d-C was higher than that of RAC-1d-C. It means the change in the bonding strength of the interface had a limited influence on the compressive strength of the concrete.

3.3.3. Stress-strain curve

The stress-strain curves of RAC prepared with different carbonation durations are presented in Fig. 16. Based on the method used in previous studies [28, [41], the secant modulus between 5 % and 1/3 peak stress was determined as the elastic modulus of the concrete. The peak stress, peak strain and elastic modulus of RAC prepared with different carbonation durations are given in Table 5. The results show that the peak stress of RAC-1h-C, RAC-1d-C, and RAC-7d-C was increased by 17.3 %, 27.4 %, and 36.5 %, respectively, and this trend was similar to that of the cube compressive strength data. The elastic modulus of RAC increased after using CRCA, but it did not show an apparent increasing trend with the increase of the carbonation duration, i.e., the elastic modulus of RAC-1h-C, RAC-1d-C, and RAC-7d-C increased by 14.7 %, 10.4 %, and 17.8 %, respectively. It might be because the denser carbonated surface layer of RCA could act as a shell to resist deformation, which played a significant role in improving the elastic modulus of RAC. After carbonation for different durations, the shell effects of RCA-1h-C, RCA-1d-C, and RCA-7d-C were similar, although their carbonation depths were different. In addition, the peak strain of RAC did not present noticeable change with the increase of carbonation duration of RCA. However, the plastic strain of RAC decreased obviously with the increase of carbonation duration of RCA. Here, the elastic strain is equal to the peak stress divided by the elastic modulus, while the plastic strain is equal to the peak strain minus the elastic strain. That was because the amount of initial microcracks in RCA were reduced after carbonation [42], which lead to less microcracks in RAC. It is well known that the plastic strain of concrete is related to the growth of microcracks [43].

3.3.4. Sorptivity

The water absorption-time curve and rate of water absorption of RAC using RCAs with different carbonation durations are shown in Fig. 17. The water absorption of RAC-control increased linearly with time before 1 day ($\sqrt{t}<294$ $s^{1/2}$). Then, the rate of increase decreased rapidly. After 5 days ($\sqrt{t}>657$ $s^{1/2}$), it only increased slightly. However, when using the RCA-1 h-C, the water absorption of the RAC-1 h-C increased approximately linearly up to 9 days ($\sqrt{t}<882$ $s^{1/2}$), while the absorption of RAC-1d-C and RAC-7d-C increased approximately linearly with time up to 16 days ($\sqrt{t}<1176$ $s^{1/2}$). From Fig. 16(b), the initial rate of absorption of RAC after using CRCA decreased significantly. However, when the carbonation duration of RCA was increased from 1 h to 7 days, the initial rate of water absorption of RAC only showed a slight decrease. That was because a denser layer (like a shell) was generated on the surface of RCA after carbonation, and it changed the path of water from “penetrating through the RCA” to “passing around the RCA”. Similar to RCA-1d-C and RCA-7d-C, RCA-1h-C also provided this shell effect. Therefore, the initial rate of water absorption only showed a slight decrease with the increase in the carbonation duration of RCA. However, the secondary rate of absorption of RAC with CRCA showed a much smaller decrease than the initial rate of absorption. That was because water only passed around CRCA when RAC was absorbing water within 1 day, but after 1 day, water began to penetrate the CRCA. It also explains why the absorption increased linearly up to 9 days for RAC-1h-C, and up to 16 days for RAC-1d-C for RAC-7d-C. In addition, the total absorption of RAC decreased with the increase in carbonation duration of RCA, as shown in Fig. 17(a). That is because the porosity of RCA decreased with the carbonation duration, which absorbed less water. But it decreased much slower after 1 h of carbonation, i.e., the total absorption of RAC-1h-C, RAC-1d-C, and RAC-7d-C was reduced by 15.6 %, 18.0 %, and 21.6 %, respectively. It indicates that the denser surface layer of CRCA played an important role in reducing the total absorption of RAC.

3.3.5. Chloride penetration resistance

The chloride penetration resistances of RAC using RCAs prepared with different carbonation durations are shown in Fig. 18. With the increase of RCA carbonation duration to 7 days, the charge passed values of the corresponding RAC decreased. Compared to RAC-control, the decreased rate of charge passed of RAC-1h-C, RAC-1d-C, and RAC-7d-C were 2.2 %, 7.8 %, and 15.8 %, respectively. From Fig. 18(b), the decreasing rate of charge passed of RAC seems to exhibit an exponential increase with the decrease of water absorption of CRCA. In the RAC prepared with CRCAs, as the new mortar was considered similar, the porosity of RAC was elated to the porosity or water absorption of CRCA. It means that the charge passed of RAC with CRCA shows an exponential increase of the porosity of RAC, which was similar to normal concrete. Generally, the amount of charge passed increases exponentially with porosity [44]. Therefore, it can be inferred that the enhancement of chloride penetration resistance of RAC was mainly dependent on the reduced porosity of

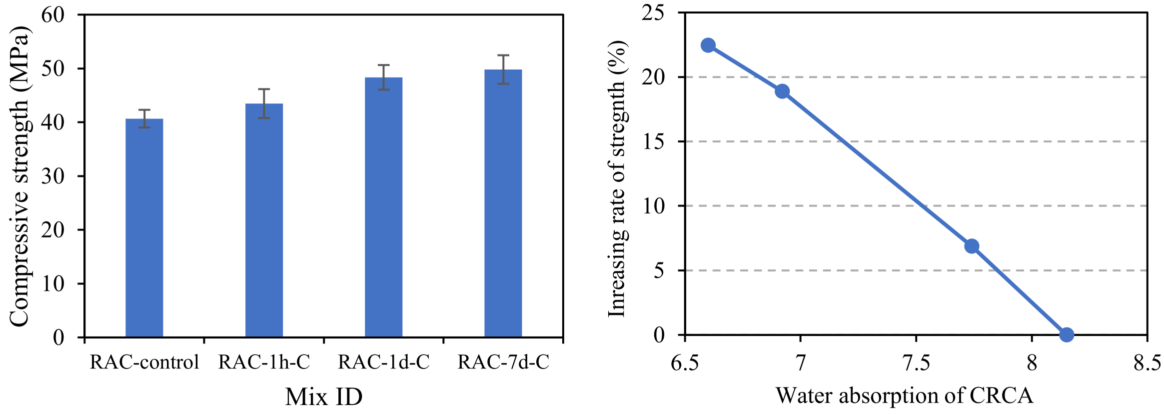

(a)   (b)

Fig. 15. Compressive strength of RAC with CRCAs (a) and the relationship of its increasing rate with water absorption of CRCA (b).

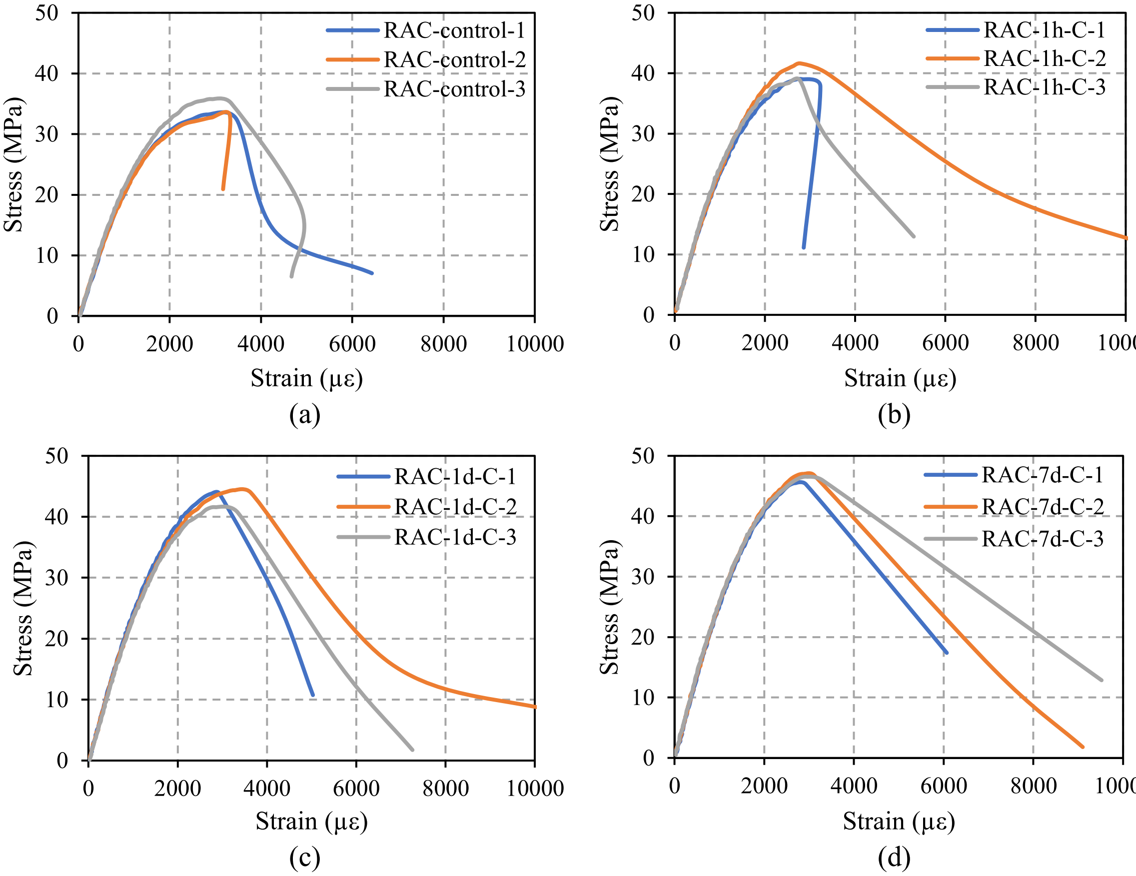

Fig. 16. Stress-strain curves of RAC using RCA with different carbonation durations. (a) RAC-control; (b) RAC-1 h-C; (c) RAC-1d-C; (d) RAC-7d-C.

CRCA, rather than on the denser surface layer of CRCA.

4. Conclusions

This study systematically investigated the effect of carbonation duration on the properties of recycled coarse aggregate (RCA), RCA-new mortar interface, and recycled aggregate concrete (RAC). Based on the results and discussion, the following conclusions could be

Table 5
Peak stress, peak strain, elastic modulus of RAC using RCA with varied carbonation durations.

Mix ID	Peak stress (MPa)	Elastic modulus (GPa)	Peak strain (με)	Elastic strain to peak strain ratio	Plastic strain to peak strain ratio
RAC-Control	33.9 (1.25)	23.4 (0.76)	2942 (270)	0.50 (0.04)	0.50 (0.04)
RAC-1h-C	39.8 (1.54)	26.8 (0.75)	2800 (30)	0.53 (0.03)	0.47 (0.03)
RAC-1d-C	43.3 (1.49)	25.8 (0.49)	3020 (229)	0.56 (0.03)	0.44 (0.03)
RAC-7d-C	46.3 (0.78)	27.5 (0.32)	2853 (136)	0.59 (0.03)	0.41 (0.03)

Note: The numbers in the bracket are standard deviations.

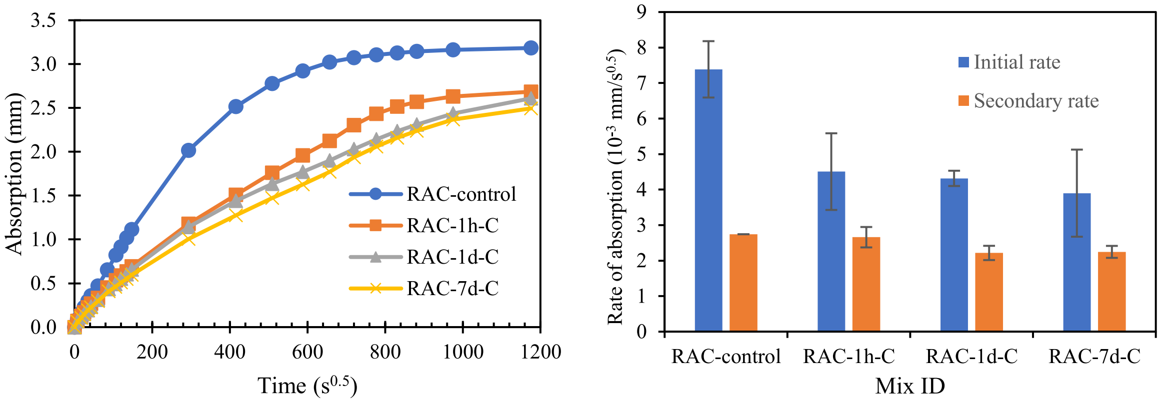

(a) (b)

Fig. 17. Absorption-time curve (a) and rate of absorption (b) of RACs using RCA with different carbonation durations.

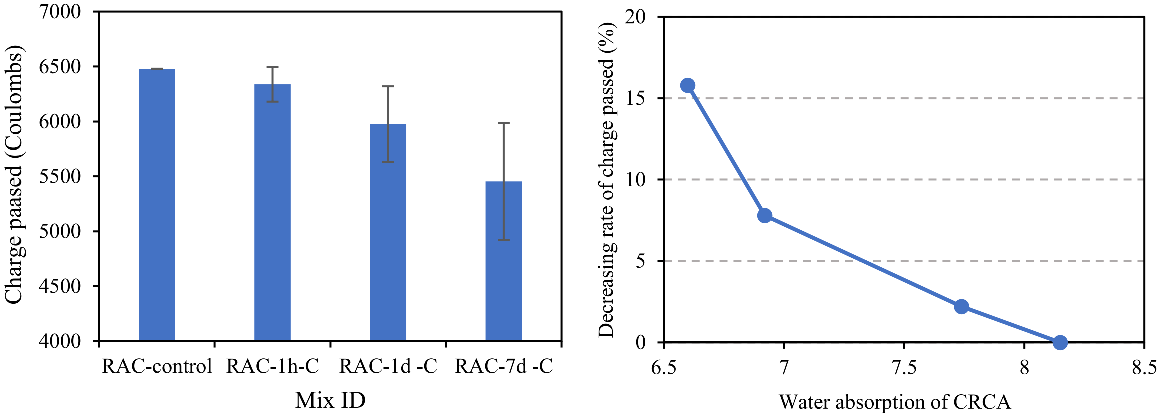

(a) (b)

Fig. 18. Charge passed of RAC with CRCAs (a) and the relationship of its decreasing rate with water absorption of CRCA (b).

made.

(1) With the increase in carbonation duration, the water absorption of RCA decreased, but it decreased at a much slower rate after 1 day of carbonation. That is because CO_2 was more difficult to diffuse into the inner part of RCA, while most of CH and Ca-rich C-S-H in RCA had already reacted with CO_2 within 1 day, and the further carbonation of Si-rich C-S-H was much slower.

(2) With the increased carbonation duration, the bonding strength of the interface between RCA and new mortar increased first and then decreased, but it had limited influence on the performance of RAC. The microhardness of the interface transition zone and the new mortar in RAC did not show obvious change when using CRCAs.

(3) The compressive strength of RAC and chloride penetration resistance increased with the increase of carbonation duration of RCA, and the enhancement are dependent on the reduction in porosity of CRCA. However, the elastic modulus of RAC increased after using CRCA, but it did not show an apparent trend with the increase of carbonation duration.

(4) The initial rate of absorption and total absorption of RAC decreased with the use of CRCA, but it decreased much slower after 1 h of carbonation. The decrease in initial absorption of water of RAC was mainly dependent on the denser surface layer of CRCA, rather than the reduced porosity of CRCA. This is because the denser surface layer can change water path from “penetrating through RCA” to “passing around RCA”.
(5) It is recommended to use 1-day pressurized carbonation of RCA to enhance RAC which would have a higher cost-effectiveness.

Declaration of Competing Interest

The authors declare that they have no known competing financial interests or personal relationships that could have appeared to influence the work reported in this paper.

Data availability

Data will be made available on request.

Acknowledgement

The authors would like to thank the Hong Kong Research Grants Council , the Innovation Technology Fund and The Hong Kong Polytechnic University for financial support.

References

[1] J.Z. Xiao, J.B. Li, Ch Zhang, Mechanical properties of recycled aggregate concrete under uniaxial loading, Cem. Concr. Res. 35 (6) (2005) 1187–1194.
[2] B. Lei, H. Yu, Y. Guo, W. Dong, R. Liang, X. Wang, X. Lin, K. Wang, W. Li, Fracture behaviours of sustainable multi-recycled aggregate concrete under combined compression-shear loading, J. Build. Eng. 72 (2023), 106382.
[3] B. Lei, L. Yu, Y. Guo, A.H. Mahmood, F. Qu, X. Wang, W. Li, Failure behaviour and damage evolution of multi-recycled aggregate concrete under triaxial compression, Eng. Fail. Anal. 153 (2023), 107572.
[4] I.B. Topçu, S. Sengel, Properties of concretes produced with waste concrete aggregate, Cem. Concr. Res. 34 (8) (2004) 1307–1312.
[5] M. Etxeberria, E. Vázquez, A. Marí, M. Barra, Influence of amount of recycled coarse aggregates and production process on properties of recycled aggregate concrete, Cem. Concr. Res. 37 (5) (2007) 735–742.
[6] C.S. Poon, Z.H. Shui, L. Lam, Effect of microstructure of ITZ on compressive strength of concrete prepared with recycled aggregates, Constr. Build. Mater. 18 (6) (2004) 461–468.
[7] A. Akbarnezhad, K.C.G. Ong, M.H. Zhang, C.T. Tam, T.W.J. Foo, Microwave assisted beneficiation of recycled concrete aggregates, Constr. Build. Mater. 25 (8) (2011) 3469–3479.
[8] H. Zhao, W. Li, Y. Gan, K. Wang, Z. Luo, Nano/microcharacterization and image analysis on bonding behaviour of ITZs in recycled concrete enhanced with waste glass powder, Constr. Build. Mater. 392 (2023), 131904.
[9] L. Li, J.Z. Xiao, D.X. Xuan, C.S. Poon, Effect of carbonation of modeled recycled coarse aggregate on the mechanical properties of modeled recycled aggregate concrete, Cem. Concr. Compos. 89 (2018) 169–180.
[10] X. Ke, D. Xu, M. Cai, Experimental and numerical study on the eccentric compressive performance of RAC-encased RACFST composite columns, Eng. Struct. 224 (2020), 111227.
[11] A. Verma, V.S. Babu, S. Arunachalam, Characterization of recycled aggregate by the combined method: Acid soaking and mechanical grinding technique, Mater. Today.: Proc. (2021).
[12] A. Akbarnezhad, K.C.G. Ong, M.H. Zhang, C.T. Tam, T.W.J. Foo, Microwave assisted beneficiation of recycled concrete aggregates, Constr. Build. Mater. 25 (8) (2011) 3469–3479.
[13] V.W.Y. Tam, C.M. Tam, K.N. Le, Removal of cement mortar remains from recycled aggregate using pre-soaking approaches, Resour. Conserv. Recycl. 50 (1) (2007) 82–101.
[14] B.J. Zhan, C.S. Poon, Q. Liu, S.C. Kou, C.J. Shi, Experimental study on CO_2 curing for enhancement of recycled aggregate properties, Constr. Build. Mater. 67 (2014) 3–7.
[15] A. Mansur, D. Santos, H. Mansur, A microstructural approach to adherence mechanism of poly (vinyl alcohol) modified cement systems to ceramic tiles, Cem. Concr. Res. 37 (2) (2007) 270–282.
[16] H. Zhang, Y. Zhao, T. Meng, et al., Surface treatment on recycled coarse aggregates with nanomaterials, J. Mater. Civ. Eng. 28 (2) (2015), 04015094.
[17] V.W.Y. Tam, X.F. Gao, C.M. Tam, Microstructural analysis of recycled aggregate concrete produced from two-stage mixing approach, Cem. Concr. Res. 35 (6) (2005) 1195–1203.
[18] V. Corinaldesi, G. Moriconi, Influence of mineral additions on the performance of 100% recycled aggregate concrete, Constr. Build. Mater. 23 (2009) 2869–2876.
[19] B.B. Mukharjee, S.V. Barai, Influence of Nano-Silica on the properties of recycled aggregate concrete, Constr. Build. Mater. 55 (2014) 29–37.
[20] C. Liang, B. Pan, Z. Ma, Z. He, Z. Duan, Utilization of CO_2 curing to enhance the properties of recycled aggregate and prepared concrete: a review, Cem. Concr. Compos. 105 (2020), 103446.
[21] J. Zhang, C. Shi, Y. Li, X. Pan, C.S. Poon, Z. Xie, Influence of carbonated recycled concrete aggregate on properties of cement mortar, Constr. Build. Mater. 98 (2015) 1–7.
[22] J. Zhang, C. Shi, Y. Li, X. Pan, C.S. Poon, Z. Xie, Performance enhancement of recycled concrete aggregates through carbonation, J. Mater. Civ. Eng. 11 (27) (2015), 04015029.
[23] B.J. Zhan, C.S. Poon, Q. Liu, S. Kou, C. Shi, Experimental study on CO_2 curing for enhancement of recycled aggregate properties, Constr. Build. Mater. 67 (2014) 3–7.
[24] S. Kou, B. Zhan, C.S. Poon, Use of a CO_2 curing step to improve the properties of concrete prepared with recycled aggregates, Cem. Concr. Compos. 45 (2014) 22–28.
[25] B.J. Zhan, D.X. Xuan, C.S. Poon, K.L. Scrivener, Characterization of interfacial transition zone in concrete prepared with carbonated modeled recycled concrete aggregates, Cem. Concr. Res. 136 (2020), 106175.
[26] J. Wang, J. Zhang, D. Cao, H. Dang, B. Ding, Comparison of recycled aggregate treatment methods on the performance for recycled concrete, Constr. Build. Mater. 234 (2020), 117366.
[27] Y. Jiang, P. Shen, C.S. Poon, Improving the bonding capacity of recycled concrete aggregate by creating a reactive shell with aqueous carbonation, Constr. Build. Mater. 315 (2022), 125733.

[28] L. Li, D. Xuan, A.O. Sojobi, S. Liu, C.S. Poon, Efficiencies of carbonation and nano silica treatment methods in enhancing the performance of recycled aggregate concrete, Constr. Build. Mater. 308 (2021), 125080.

[29] N. Russo, F. Lollini, Effect of carbonated recycled coarse aggregates on the mechanical and durability properties of concrete, J. Build. Eng. 51 (2022), 104290.

[30] R. Neves, F. Branco, J. de Brito, Field assessment of the relationship between natural and accelerated concrete carbonation resistance, Cem. Concr. Compos. 41 (2013) 9–15.

[31] S. Steiner, B. Lothenbach, T. Proske, A. Borgschulte, F. Winnefeld, Effect of relative humidity on the carbonation rate of portlandite, calcium silicate hydrates and ettringite, Cem. Concr. Res. 135 (2020), 106116.

[32] P. Shen, Y. Zhang, Y. Jiang, B. Zhan, J. Lu, S. Zhang, C.S. Poon, Phase assemblance evolution during wet carbonation of recycled concrete fines, Cem. Concr. Res. 154 (2022), 106733.

[33] X. Liu, P. Feng, Y. Cai, X. Yu, C. Yu, Q. Ran, Carbonation behavior of calcium silicate hydrate (C-S-H): Its potential for CO_2 capture, Chem. Eng. J. 431 (2022), 134243.

[34] F. Bosch Reig, J.V. Gimeno Adelantado, M.C.M. Moya Moreno, FTIR quantitative analysis of calcium carbonate (calcite) and silica (quartz) mixtures using the constant ratio method. Application to geological samples, Talanta 58 (4) (2002) 811–821.

[35] D. Chakrabarty, S. Mahapatra, Aragonite crystals with unconventional morphologies, J. Mater. Chem. 9 (11) (1999) 2953–2957.

[36] E. Loftus, K. Rogers, J. Lee-Thorp, A simple method to establish calcite: aragonite ratios in archaeological mollusc shells, J. Quat. Sci. 30 (2015) 731–735.

[37] J.D. Rodriguez-Blanco, S. Shaw, L.G. Benning, The kinetics and mechanisms of amorphous calcium carbonate (ACC) crystallization to calcite, via vaterite, Nanoscale 3 (1) (2011) 265–271.

[38] E.A.A. Versteegh, S. Black, M.E. Hodson, Carbon isotope fractionation between amorphous calcium carbonate and calcite in earthworm-produced calcium carbonate, Appl. Geochem. 78 (2017) 351–356.

[39] B.J. Saikia, G. Parthasarathy, N.C. Sarmah, Fourier transform infrared spectroscopic estimation of crystallinity in SiO2 based rocks, Bull. Mater. Sci. 31 (5) (2008) 775–779.

[40] L. Li, J. Lu, P. Shen, K. Sun, L.E.L. Pua, J. Xiao, C.S. Poon, Roles of recycled fine aggregate and carbonated recycled fine aggregate in alkali-activated slag and glass powder mortar, Constr. Build. Mater. 364 (2023), 129876.

[41] L. Li, D.X. Xuan, S.H. Chu, C.S. Poon, Modification of recycled aggregate by spraying colloidal nano silica and silica fume, Mater. Struct. 54 (2021) 223.

[42] L. Li, C.S. Poon, J. Xiao, D. Xuan, Effect of carbonated recycled coarse aggregate on the dynamic compressive behavior of recycled aggregate concrete, Constr. Build. Mater. 151 (2017) 52–62.

[43] A. Dragon, Z. Mróz, A continuum model for plastic-brittle behaviour of rock and concrete, Int. J. Eng. Sci. 17 (2) (1979) 121–137.

[44] M.H. Nguyen, V.T. Nguyen, T.P. Huynh, C.L. Hwang, Incorporating industrial by-products into cement-free binders: Effects on water absorption, porosity, and chloride penetration, Constr. Build. Mater. 304 (2021), 124675.